Identification of cracks in box-section beams with a cracked beam element model

IDENTIFICATION OF CRACKS IN BOX-SECTION BEAMS WITH A CRACKED BEAM ELEMENT MODEL

Chuanchuan HOU [1] and Yong LU [2]

ABSTRACT

Box-section steel members are widely used in different types of engineering structures. Identification of cracks in box-section members poses a particular challenge because of the section geometry. This paper presents a crack identification approach for box-section beam-column members based on a cracked beam element model and using a finite element model updating procedure. The cracked beam element model is established by involving an additional local flexibility due to the crack, which is formulated using the fracture mechanics principles. To calculate the additional local flexibility, the stress intensity factors for cracks in box sections need to be established and this is achieved using an empirical approach combining FE simulation, parametric analysis and regression. The cracked beam element model is verified in terms of its predictions of the dynamic properties of cracked box-section beams against both FE simulated and experimentally measured modal data. Both thick-walled and thin-walled box-section beams have been considered in the FE simulated examples, while several box-section beams with different numbers of cracks have been tested in the experiment. Subsequently, the model is incorporated in the crack damage identification procedure. Results indicate that cracks can be identified correctly for beams with both single crack and multiple cracks and the identified crack parameters are of good accuracy.

Keywords: Box-section beam, dynamic properties, damage identification, cracked beam element, model updating, modal testing

[1] Ph.D. Student, Institute for Infrastructure and Environment, School of Engineering, the University of Edinburgh, Edinburgh EH9 3JL, UK. E-mail: c.hou@ed.ac.uk

[2] Professor, Institute for Infrastructure and Environment, School of Engineering, the University of Edinburgh, Edinburgh EH9 3JL, UK (corresponding author). E-mail: yong.lu@ed.ac.uk

INTRODUCTION

Box section beams have been widely used in different types of engineering structures, from large-size box girders in bridge structures, medium-size beams and columns in buildings, to small-size vehicle frames. The main advantage of box section members is that sufficient bending and torsion stiffness can be achieved while the self-weight of the structure is greatly reduced. Box beams with small wall thickness belong to thin-walled members, and have been extensively studied since Vlasov (1961). In the service life of box beams, one critical issue is the development of cracks in the beam walls. One example is the development of fatigue crack of steel box beams under cyclic loading, especially at the welding locations (Nussbaumer et al., 1999). Identification of the occurrence of cracks is thus an important topic for the monitoring and maintenance of box beam structures.

Among various types of techniques for structural health monitoring, vibration-based damage identification is one of the most researched approaches (Doebling et al., 1996; Mottershead and Friswell, 1993; Sohn et al., 2004). This approach employs measured modal data to identify the existence, location and severity of damages in the structures. In the past, vibration-based damage identification has been applied on various types of structures, such as RC beams (Cerri and Vestroni, 2003; Unger et al., 2006), composite beams (Moaveni et al., 2008), and steel space structures like frame or truss (Hu et al., 2001; Jones and Turcotte, 2002; Lu and Tu, 2004).

It is noted that most of the studies have dealt with solid section members, such as concrete beams, or solid steel members in space structures. Limited research has been devoted to crack damage identification of hollow section structures. Of the few relevant publications, two are summarized here. Liu et al. (2003) studied the crack detection in hollow circular section beams. The crack detection method is based on the fact that a circumferential crack in a hollow section brings coupled vibration between longitudinal and bending vibrations, and

thus an extra resonant peak appears in the frequency response function of the cracked beam. This method is capable of detecting the existence of cracks, but it is difficult to predict the severity (crack depth) and location parameters, especially when multiple cracks exist. Zheng and Fan (2003) analysed the vibration of cracked hollow section beams with circular or square sections. The vibration functions were established by treating the cracked beams as an assembly of sub-segments linked up by rotational springs. The stiffness of the rotational springs was expressed with some local flexibility coefficients for the cracks, which were derived from fracture mechanics principles. It is noted that in the above study the stress intensity factors (SIFs) for cracks in plane sections were employed for the local flexibility calculation of hollow sections, and this treatment could bring in marked errors as cracks in hollow sections is a three-dimensional problem in nature and specific SIFs for this type of sectional configuration should be used.

The present paper is aimed for the crack identification of box section beams with a suitable cracked element description for this type of structural members. The general identification adopts a model-based approach, in which a structural model (finite element model) is employed and the variable model parameters are updated in accordance with the measured modal data. In order for the crack parameters to be identified accurately through this procedure, first a cracked beam element model is developed for the cracked box-section beams with explicit descriptions of the crack parameters, including the crack severity (depth) and its relative location within an element. The cracked beam element is established through incorporating an additional local flexibility brought by the crack, which is in turn related to the stress intensity factors (SIFs) for box-section beams. A general formulation is presented for the additional local flexibility for generic box sections. Am empirical procedure is adopted for the derivation of the SIFs combining FE simulation, parametric analysis and regression. Specific SIF results are obtained for square box sections to demonstrate the empirical

74 procedure and subsequently to verify the cracked beam element model. The verification is
75 firstly carried out in the (forward) prediction of the modal properties, particularly natural
76 frequencies and mode shapes, using the cracked box section beam element model against
77 refined finite element simulations. The cracked beam element is then incorporated in a model
78 updating procedure for crack identification. Finally the cracked beam element model and the
79 crack identification procedure are applied on experimental square box beams with different
80 configurations of cracks.

81 CRACKED BEAM ELEMENT MODEL FOR BOX-SECTION BEAMS

82 Various simplified crack models have been developed in the literature for the vibration
83 analysis of cracked beams. Generally speaking the models may be divided into four categories,
84 namely a) reduced stiffness model, b) models based on stress fields, c) models based on a
85 discrete spring scheme, and d) models based on local flexibility and fracture mechanics. A
86 recent study by the authors (Hou and Lu, 2016) on relatively thick cracked beams whose
87 length to depth ratio is around 10 shows that a cracked beam element model formulated on the
88 basis of additional flexibility and fracture mechanics has superior performance over other
89 models in two important aspects, 1) the model is capable of providing a consistent and
90 accurate representation of the effect of a crack on the vibration properties of a cracked beam
91 for practically all modes of interest; 2) the model takes into account specific features
92 concerning the vibration of thick beams, including shear deformation and coupling between
93 the flexural and longitudinal modes. In contrast, the reduced stiffness model, which is widely
94 used in the damage identification literature, is incapable of maintaining a consistent
95 representation of the crack effect for different modes. So in the present study the cracked
96 beam element model has been adopted and extended to model the cracked box section beams.

97 One-dimensional beam element for intact box-section beams

Usually a cracked beam element model is formulated as an extension from the respective intact beam element model by incorporating the influence of cracks. For the box section beams, first a suitable one-dimensional beam element for the intact box beams is selected. The classic Euler-Bernoulli and Timoshenko beam elements are general choices for modelling beam-like structures. These beam elements can also be adopted for modelling box-section beams. However, it is known that for relatively thin-walled box beams under loading, in-plane deformations such as warping, distortion and shear-lag effect cannot be ignored. The plane section assumption for classic beam elements does not strictly hold for box sections due to these effects. Consequently, marked modelling errors could arise when using classic beam models for box beams. To overcome this issue, some advanced one-dimensional beam elements have been developed in the past to account for the warping, distortion or shear-lag effects in thin-walled box beams. Some representative models are summarized here.

Carrera et al. (2011), Carrera and Varello (2012) developed a refined beam theory for thin-walled structure with in-plane stretching considered. The obtained beam element has 9 degrees of freedom at each node, resulting in an 18×18 stiffness matrix. Kim and Kim (1999) developed a two-noded C^0 continuous thin-walled box beam element with the coupled deformation of torsion, warping and distortion considered. At each node, the axial rotation, warping, and distortion are used as degrees of freedom, and the resulted stiffness and mass matrices are of size 6×6. Another group of one-dimensional beam elements incorporate the shear-lag effect in the bending analysis of box girders (Luo et al., 2002; Zhang and Lyons, 1984; Zhang and Lin, 2014; Zhou, 2010). These models used the assumption by Reissner (1946) of a displacement function for shear lag warping to obtain the shear-lag induced axial stress distribution. The beam stiffness matrix can be obtained from the strain energy of the beam element, in which the shear-lag induced rotation is generally used as an independent degree of freedom. As a result, the size of the stiffness matrix will be expanded compared to

123 the stiffness matrix from classical Euler-Bernoulli or Timoshenko theory and the bending
124 stiffness of the beam model is reduced due to the existence of shear-lag effect.

125 The present study is mainly concerned about crack identification for box-section beams.
126 To simplify the formulation while retaining the essential effect of cracks, the classic
127 Timoshenko beam element is selected for the modelling of intact box beams and forms the
128 basis for the cracked beam element model. It can be readily replaced with a more advanced
129 beam model as mentioned above and the formulation procedure is similar to what is discussed
130 in this paper. But as will be shown later in the application (numerical) and experimental
131 verification sections, the Timoshenko-based cracked beam element model is sufficiently
132 effective for crack identification of box beams with either relatively thick or thin walls.

133 **Crack model formulation**

134 The additional flexibility for the cracked box section beam is established using the energy
135 approach in conjunction with the fracture mechanics theory. Let a generic box section size be
136 $B \times D$, as shown in Fig. 1. The wall thicknesses for the horizontal and vertical walls are t_{sB} and
137 t_{sD}, respectively. Assume that fracture of the beam is due to vertical bending and the crack
138 starts from the centre of bottom edge and propagates symmetrically towards the corners with
139 a length of a_H ($\leq B/2$), which is defined as Stage 1 of the crack development. After the whole
140 bottom wall is cracked, the crack goes up to the side walls with a depth of a_V ($\leq D$), defined as
141 Stage 2.

142 A cracked box beam element with 6 degrees of freedom (DOFs) in the x-y plane is
143 developed to model the box beam with a cracked section shown in Fig. 1. The DOFs consist
144 of axial, transverse and rotational DOFs but without torsion, as shown in Fig. 2. The element
145 has a length of l_e and the crack is located at a distance of l_c from the left node. In Stage 1 of
146 the crack propagation, the total crack length a can be calculated as $2a_H$, and in Stage 2 as
147 $B+2a_V$. A crack length ratio is defined as the ratio of a_H to the width B, $\alpha_H = a_H/B$ ($\alpha_H \leq 0.5$).

148 Similarly, a crack depth ratio for the crack in the vertical walls is defined as $\alpha_V = a_V/D$ ($\alpha_V \leq$

149 1.0). An overall crack depth ratio α is further defined as,

150 $$\alpha = \begin{cases} \alpha_H & \text{when crack is only in the bottom wall} \\ 0.5 + \alpha_V & \text{when crack propages into vertical walls} \end{cases} \quad (1)$$

151 The strain energy in the cracked beam element under a generalised load is equal to the

152 strain energy of the intact beam element plus the additional strain energy brought by the crack,

153 as shown in Eq. (2). The additional strain energy due to the presence of a crack can be

154 evaluated by the fracture energy. Let the element be subjected to axial load P (u), shear force

155 Q (v) and bending moment M (θ).

156 $$U_T = U_0 + U_c \quad (2)$$

157 The additional strain energy brought by the crack U_c can be established according to the

158 fracture mechanics theory as equal to the fracture energy:

159 $$U_c = \int_{A_c} G \mathrm{d}A \quad (3)$$

160 where, G is the energy release rate and A_c is the effective crack area. The relationships

161 between the energy release rate G and the stress intensity factors (SIFs) are shown in Eq. (4)

162 (Tada et al., 2000).

163 $$G = \frac{1}{E'}\left(K_I^2 + K_{II}^2 + \frac{1}{1-\nu} K_{III}^2 \right) \quad (4)$$

164 where K_I, K_{II} and K_{III} are the stress intensity factors for the open, sliding and tearing cracks,

165 respectively; For plane stress, $E'=E$, and for plane strain, $E'=E/(1-\nu)$, where ν is the Poisson's

166 ratio of the material.

167 For the cracked beam element considered in Fig. 2, only the first SIF K_I needs to be

168 considered for crack in Stage 1 whereas only the first two SIFs, K_I and K_{II}, exists for Stage 2.

169 As the beam wall thickness is relatively thin, the crack problem is treated as plane stress.

170 The formulations of the first two types of SIFs can be expressed as (Liu, 1996; Tada et al.,

2000):

$$K_{\mathrm{I1}} = \frac{P}{A_0}\sqrt{\pi a}F_{\mathrm{I1}}(a,...) \tag{5a}$$

$$K_{\mathrm{I2}} = \frac{MD}{2I}\sqrt{\pi a}F_{\mathrm{I2}}(a,...) \tag{5b}$$

$$K_{\mathrm{II}} = \frac{Q}{A_{\mathrm{e}}}\sqrt{\pi a}F_{\mathrm{II}}(a,...) \tag{5c}$$

where, K_{I1} and K_{I2} are the SIFs of mode I crack under axial loading and pure bending, respectively; K_{II} is the SIF of mode II under shear loading. A_0 is the sectional area of the box beam; I is the second moment of area of the box section; A_{e} is the effective shear area of the box beam section, which can be calculated as $A_{\mathrm{e}}=\kappa A_0$ and the shear coefficient κ for box beam is calculated with the equation recommended by Cowper (1966):

$$\kappa = \frac{10(1+\nu)(1+3m)^2}{(12+72m+150m^2+90m^3)+(11+66m+135m^2+90m^3)\nu+10n^2((3+\nu)m+3m^2)} \tag{6}$$

where, $m=(B-2t_{\mathrm{sD}})t_{\mathrm{sB}}/(Dt_{\mathrm{sD}})$, $n=(B-2t_{\mathrm{sD}})/D$.

There are three dimensionless terms FI1, FI2 and FII in Eq. (5), which are functions of geometrical parameters of the section and crack depth. Expressions for these terms will be presented in the next sub-section.

With Eq. (4) and (5), the strain energy release rate G for the current loading case can be written as:

For crack development in Stage 1,

$$G = \frac{1}{E}\left(\frac{P}{A_0}\sqrt{\pi a_{\mathrm{H}}}F_{\mathrm{I1}}^{\mathrm{H}} + \frac{D(M+Ql_e-Ql_c)}{2I}\sqrt{\pi a_{\mathrm{H}}}F_{\mathrm{I2}}^{\mathrm{H}}\right)^2 \tag{7a}$$

where $F_{\mathrm{I1}}{}^{\mathrm{H}}$ and $F_{\mathrm{I2}}{}^{\mathrm{H}}$ are terms related to cracks in Stage 1 .

For crack development in Stage 2,

$$G = \frac{1}{E}\left[\left(\frac{P}{A_0}\sqrt{\pi a_{\mathrm{V}}}F_{\mathrm{I1}}^{\mathrm{V}} + \frac{D(M+Ql_e-Ql_c)}{2I}\sqrt{\pi a_{\mathrm{V}}}F_{\mathrm{I2}}^{\mathrm{V}}\right)^2 + \left(\frac{Q}{A_{\mathrm{e}}}\sqrt{\pi a_{\mathrm{V}}}F_{\mathrm{II}}^{\mathrm{V}}\right)^2\right] \tag{7b}$$

where F_{I1}^{V}, F_{I2}^{V} and F_{II}^{V} are terms related to cracks in Stage 2.

The strain energy of an intact Timoshenko beam element U_0 can be calculated as:

$$U_0 = \frac{1}{2}\int_0^{l_e}\left[\frac{(M+Ql_e-Qx)^2}{EI}+\frac{Q^2}{GA_e}+\frac{P^2}{EA_0}\right]\mathrm{d}x \tag{8}$$

With the total strain energy of the cracked beam, the flexibility can then be obtained by invoking Castigliano's theorem as:

$$c_{ij} = \frac{\partial U_T}{\partial F_i \partial F_j} = \frac{\partial U_0}{\partial F_i \partial F_j} + \frac{\partial U_c}{\partial F_i \partial F_j} \tag{9a}$$

$$\text{or} \qquad c_{ij} = c_{ij,0} + c_{ij,c} \tag{9b}$$

where, c_{ij} is the total local flexibility and F_i is the force applied on the i^{th} DOF of the beam node. $c_{ij,0}$ is the flexibility of the intact beam element, and $c_{ij,c}$ is the additional flexibility due to the presence of the crack.

With Eq. (7), (8) and (9), the additional flexibility for the cracked beam element can be calculated as:

For crack only in Stage 1:

$$c_{ij,c} = \frac{2\partial^2}{\partial F_i \partial F_j}\int_0^{a_H}\frac{t_{sB}}{E}\left[\left(\frac{P}{A_0}\sqrt{\pi a}F_{I1}^{H}+\frac{D(M+Ql_e-Ql_c)}{2I}\sqrt{\pi a}F_{I2}^{H}\right)^2\right]\mathrm{d}a \tag{10a}$$

For crack goes into Stage 2:

$$\begin{aligned} c_{ij,c} = {} & \frac{2\partial^2}{\partial F_i \partial F_j}\int_0^{0.5B}\frac{t_{sB}}{E}\left[\left(\frac{P}{A_0}\sqrt{\pi a}F_{I1}^{H}+\frac{D(M+Ql_e-Ql_c)}{2I}\sqrt{\pi a}F_{I2}^{H}\right)^2\right]\mathrm{d}a \\ & + \frac{2\partial^2}{\partial F_i \partial F_j}\int_0^{a_V}\frac{t_{sD}}{E}\left[\left(\frac{P}{A_0}\sqrt{\pi a}F_{I1}^{V}+\frac{D(M+Ql_e-Ql_c)}{2I}\sqrt{\pi a}F_{I2}^{V}\right)^2+\left(\frac{Q}{A_e}\sqrt{\pi a}F_{II}^{V}\right)^2\right]\mathrm{d}a \end{aligned} \tag{10b}$$

where, i, j = 1, 2, 3, and F_1=P, F_2=Q, F_3=M.

It can be seen that there are 2 parameters representing explicitly the crack information in c_{ij}, namely crack depth a and crack location l_c.

The complete 6×6 stiffness matrix for the element can be obtained by inverting the

flexibility matrix and satisfying the force equilibrium in the elements, as follows:

$$\mathbf{K}_c = \mathbf{T} * \mathbf{C}^{-1} * \mathbf{T}^T \tag{11}$$

where **C** is the 3×3 flexibility matrix with c_{ij} as its elements. **T** is the transformation matrix,

$$T = \begin{bmatrix} -1 & 0 & 0 \\ 0 & -1 & 0 \\ 0 & -l_e & -1 \\ 1 & 0 & 0 \\ 0 & 1 & 0 \\ 0 & 0 & 1 \end{bmatrix} \tag{12}$$

Stress intensity factors (SIFs) for cracked square box beams

To calculate the additional flexibility in Eq. (10), the SIFs for box section beams are required. The SIFs are defined to represent the strength of the stress fields surrounding the crack-tip and are determined by the boundaries of the cracked body and loads imposed (Tada et al., 2000). SIFs for plane problems have been well established in the past, such as in the handbook by Tada et al. (2000). For members with a 3D geometry however, the solutions are always case-dependent as the shape of the 3D structures can be quite complicated. In the past several decades, many studies have tried to obtain the SIFs for various 3D structures, using methods such as the boundary collocation method and the finite element methods. Some studies have also tried to get simplified SIF models for thin-walled structures (Gao and Herrmann, 1992; Xie et al., 2004). But most of those models mainly focus on the first type (open) crack. Among various types of methods, the FE modelling approach is an effective and straightforward way for the estimation of SIFs. With proper model setting, highly accurate SIFs can be extracted from FE analysis (Carpinteri et al., 2006; Dunn et al., 1997; Wang et al., 2005)

To obtain a full list of SIFs for both open and sliding cracks in both development stages of a cracked box section beam, FE modelling approach is adopted in this study to establish the

SIF formulations. The values of SIFs are calculated from FE modelling for cracked box sections with varying geometrical parameters. With parametric analysis, the main parameters that may influence the SIFs are determined. Subsequently, a regression analysis is applied to establish empirical formulas for the SIFs.

Commercial FE package ABAQUS is used to generate the SIF values for crack box beams. As a special type of box section, herein a square box beam with uniform wall thickness is used as an example. Other types of sections, such as rectangular box section or sections with non-uniform wall thickness, can be applied with the same procedure. The box beam is simulated with 4-node shell element with reduced integration (S4R). To precisely model the crack behaviour, a series of ring meshes are applied around the crack tip, as shown in Fig. 3. A mesh convergence check has been conducted to confirm that the finally adopted mesh is sufficiently accurate as far as mesh is concerned.

In order to deal with the singularity of stress and strain fields at the crack tip, the 'degenerate element control' command in ABAQUS is used at the crack tip. To output the stress intensity factors of the structure, the 'Contour integral evaluation' command, which could calculate the J-integral in fracture mechanics, is used in the FE model. Once the cracks are defined, both the mode I and mode II SIFs can be directly output by the software.

The dimensionless terms as defined in Eq. (5) are studied with parametric analysis. Parameters that may influence the SIFs include crack length (a_H or a_V), wall thickness to sectional width ratio (t_s/B), and sectional width (B). The following parameter ranges are considered: t_s/B= 0.02-0.1; a_H= 0-B/2; a_V= t_s-B/2, and B= 20-200 mm. As will be seen in what follows, the absolute value of B is not actually important after normalisations with respect to B.

The parametrical analysis results for dimensionless term F^V_{I2} in Stage 2 are shown in Fig. 4. It can be seen that F^V_{I2} is quite sensitive to a_V/B and t_s/B, whereas is almost constant under

different B values. Consequently, F^{V}_{I2} can be expressed as:

$$F^{V}_{I2} = F^{V}_{I2}\left(a_V/B, t_s/B\right) \tag{13}$$

A regression analysis is then carried out to obtain the expression for Eq. (13). The parametric study results show that a linear function can be used to describe the F^{V}_{I2} versus t_s/B relationship while a quartic function is suitable for the F^{V}_{I2} versus a_V/B relationship, as shown in Eq. (14).

$$F^{V}_{I2} = m\left(a_V/B\right)\cdot\left(t_s/B\right) + n\left(a_V/B\right) \tag{14}$$

where,

$$m\left(a_V/B\right) = -12.151 + 57.042\left(a_V/B\right) - 215.499\left(a_V/B\right)^2 + 376.957\left(a_V/B\right)^3 - 267.067\left(a_V/B\right)^4$$

$$n\left(a_V/B\right) = 5.269 - 24.092\left(a_V/B\right) + 100.185\left(a_V/B\right)^2 - 182.504\left(a_V/B\right)^3 + 138.946\left(a_V/B\right)^4$$

Comparisons of K^{V}_{I2} of Stage 2 from FE modelling and Eq. (14) predictions are shown in Fig. 5. It can be seen that the results match quite well with each other, with errors smaller than 1%.

Other SIF terms can be obtained with the same approach and the complete results of SIF equations are listed in the Appendix. With the SIF equations, the flexibility matrix for the cracked beam element as presented in Eq. (10) can be calculated.

APPLICATION OF THE CRACKED BEAM ELEMENT IN VIBRATION ANALYSIS AND CRACK DAMAGE IDENTIFICATION

The established cracked beam element model is first verified with numerically simulated examples. Both forward prediction for modal data and inverse crack damage identification via model updating are carried out with the cracked beam element model.

Vibration analysis with the cracked beam element

The performance of the cracked beam element for box-section beam in the prediction of the beam vibration properties, particularly the natural frequencies and mode shapes, is verified with numerical examples. Square box beams with uniform wall thickness are used as examples in the verification. At this juncture, it is worth noting that the sensitivity of the cracked beam element depends only upon the severity of a crack as measured by the additional flexibility, irrespective of the section configurations such as the aspect ratio. Therefore, by varying the degree of the crack severity in the examples with the square box section beams, the sensitivity of the crack identification method to the crack/section configurations is generally covered.

A square box beam with dimension as $B \times t_s \times L = 100 \times 10 \times 2000$ mm, as shown in Fig. 6, is simulated. The beam section has a t_s/B ratio of 0.1. The basic material properties are set as: $E = 201$ GPa, $\rho = 7850$ kg/m^3, $\nu = 0.3$. The boundary condition of the beam is set to be cantilever. The crack is set at $L_c = 600$ mm from the fixed end of the beam and assumed to have the form as shown in Fig. 1(b). Two crack depth ratios, $\alpha = 0.8$ and 1.0 (i.e., $\alpha_V = 0.3$ and 0.5), are used in the calculations. The FE model established with shell elements in the previous section is used to generate numerically simulated modal data for the intact and cracked beams. Only transverse bending modes in the simulation results are selected and applied in the following calculation.

In the beam element models, 5 Timoshenko beam elements, including 4 intact and 1 cracked, are used. Timoshenko stiffness and mass matrices with high-accuracy cubic shape functions are used for the intact elements, while the cracked beam element model described in the previous section is used for the cracked element. The cracked element is the 2nd element and the distance of the crack to the left end of the cracked element is $l_c = 200$ mm. The natural frequencies and mode shapes for the transverse modes are predicted with the beam element model (to be referred to as 'predicted') and the results are compared with the refined FE

model as discussed below.

Table 1 summarises the comparison between the numerically simulated and the predicted lowest four natural frequencies. The relative differences between the simulated and predicted frequencies are included as ε in percent. Results show that the beam element models predict the first couple modes of frequencies very accurately for both the intact and cracked beams. The 3rd and 4th modes have larger but still reasonable errors in the predicted absolute results (1.5-4.8%). At this juncture it is important to note that, as far as the identification of cracks is concerned, it is the relative shift of the modal properties from the intact state that is of most interest, not the absolute values. By examining the relative shift the inherent model error of using the Timoshenko beam representation will be largely neutralised, as discussed in what follows.

The relative shift of the natural frequency brought by the crack, S_i, is thus employed to benchmark the effectiveness of the cracked beam element model:

$$S_i = \frac{f_i^0 - f_i^{\mathrm{d}}}{f_i^0} \times 100\% \tag{15}$$

where f^0_i and f^{d}_i are the i^{th} natural frequencies of the intact and cracked beams, respectively.

Fig. 7 shows the comparison between numerically simulated and predicted frequency shifts of the beams. It can be seen that good matches are achieved for all the four modes with the relative frequency shift measure.

The accuracy of the cracked beam element model for prediction of mode shapes is examined with the Modal Assurance Criterion (MAC), as:

$$\mathrm{MAC}_i = \frac{\left(\boldsymbol{\phi}_{\mathrm{m}i}^{\mathrm{T}} \boldsymbol{\phi}_{\mathrm{c}i}\right)^2}{\left(\boldsymbol{\phi}_{\mathrm{m}i}^{\mathrm{T}} \boldsymbol{\phi}_{\mathrm{m}i}\right)\left(\boldsymbol{\phi}_{\mathrm{c}i}^{\mathrm{T}} \boldsymbol{\phi}_{\mathrm{c}i}\right)} \tag{16}$$

where, $\boldsymbol{\phi}_{\mathrm{m}i}$ and $\boldsymbol{\phi}_{\mathrm{c}i}$ are the numerically simulated (representing "measured") and the predicted i^{th} mode shapes of the cracked beam, respectively.

The obtained MAC results for the first 4 mode shapes are between 0.998 to 1.0 (hence

329 details are not shown here) and these indicate that there is almost a perfect match between the
330 numerically simulated and predicted mode shapes.

331 It should be mentioned that in the above example the crack location happens to be in the
332 middle of a cracked element. In fact the results are not very sensitive to the crack location (l_c);
333 as will be demonstrated in the experimental cases later, where single and multiple cracks take
334 place at random locations within the respective elements in the FE models, the results are
335 generally of good accuracy. Nevertheless, care should be taken in an identification procedure
336 if the crack location is found to be too close to one end of a cracked element, and this will be
337 discussed further in the next sub-section.

338 **Crack damage identification using the cracked beam element model**

339 The cracked beam element model is subsequently used for crack identification in the
340 beams. The crack identification is carried out via a finite element model updating procedure.
341 The beam element model established in the previous sub-section is adopted for updating. For
342 generality each element in the beam model is considered as a potential cracked element and is
343 modelled using the cracked beam element with both crack depth ratio (α) and location (l_c)
344 unknown. Therefore there is no limit on the number and location of cracks to be identified in
345 the beams. In the present model there are 5 beam elements in the model, thus 10 unknown
346 crack parameters need be updated. It is noted that the beam element close to the tip (free end)
347 of the cantilever beam has relatively small curvature in the vibration modes and hence will be
348 insensitive concerning the modal data. To avoid ill-conditioning, and considering that crack
349 damage does not usually occur near the free end of a cantilever beam, the free-end element is
350 excluded from the updating and assumed to be intact, leaving 8 parameters to be determined
351 from the updating.

352 An objective function incorporating the lowest four modes of eigenvalue and mode shape
353 data is used for the updating, as shown in Eq. (17).

$$J = \frac{1}{N_{\mathrm{m}}} \sum_{i=1}^{N_{\mathrm{m}}} W_i \cdot \mathrm{abs}\left(\frac{\lambda_{\mathrm{m}i}^{\mathrm{d}}}{\lambda_{\mathrm{m}i}^{0}} - \frac{\lambda_{\mathrm{c}i}^{\mathrm{d}}}{\lambda_{\mathrm{c}i}^{0}} \right) + \frac{1}{N_{\mathrm{s}} N_{\mathrm{n}}} \sum_{i=1}^{N_{\mathrm{s}}} V_i \cdot \left(\sum_{j=1}^{N_{\mathrm{n}}} \mathrm{abs}\left(\varphi_{\mathrm{m}ji}^{\mathrm{d}} - \varphi_{\mathrm{c}ji}^{\mathrm{d}} \right) \right) \tag{17}$$

where, J is the objective function to be minimised, λ denotes the eigenvalue (= $(2\pi f)^2$), φ denotes the mode shape displacement, with the subscript 'm' indicating numerically simulated data and 'c' computed data, and the superscript 'd' indicating damaged (current) state and '0' the intact state. N_{f} (= 4) is the number of eigenvalues to be included, N_{s} (= 4) is the number of mode shapes to be included, N_{n} (= 5) is the number of nodes in the mode shapes. W_i and V_i are the weights for the i^{th} eigenvalue and mode shape, respectively. As the modelling errors in the modal data tend to increase with mode number, lower weights should be assigned to higher modes. In the updatings here the weights W_i and V_i are set to be inversely proportional to the mode order, i.e. equal to $1/i$, with i= 1, 2, 3 and 4.

Genetic algorithm (GA) is employed to search for the optimal solution in the model updating (Perera and Torres, 2006; Tu and Lu, 2008). GA is a global searching engine and the searching results do not depend on the initial setting of updating parameters. It also avoids calculating the sensitivity matrix during the updating. Herein the GA function in Matlab is employed and the basic parametric settings for the GA are listed in Table 2.

The updating results of the four cracked beams are given in Fig. 8. It can be seen that the cracked element is identified correctly for both beams (element 2 in both cases), and the errors in the crack depth ratios (α) are in the range of 0.3%-2.7%. The errors in the relative location (l_c) within the cracked element are also small; the updated l_{c} values are 207mm and 209mm for the two beams, respectively, as compared to the actual 200 mm. The results suggest that the cracked beam element model is effective in the crack damage identification of box section beams.

As mentioned in the previous sub-section, in conjunction with the cases included in the experimental study later, it can be stated that the accuracy of the cracked element model is not

very sensitive to the location of the crack. Nevertheless, care should be taken in an identification application if the relative location of a crack is found to be very close to one end of a cracked element. A likely outcome in such a situation would be that both the actual cracked element and the adjacent element are identified as "cracked". To deal with this situation, a simple way is to repeat the identification (model updating) procedure with an adjusted discretization scheme. In the adjusted discretization the "suspected" crack location can be made to situate around the centre of an element to ensure the best accuracy. Further information about such an adaptive discretization procedure can be found in Hou and Lu (2016).

Performance of the cracked beam element model on thin-walled box section beams

The beam example presented in the previous section has a t_s/B ratio of 0.1, which can be categorized as a thick-walled beam. Results show that the cracked beam element model performs well for both vibration property predictions and crack damage identification of the thick-walled cases.

In applying the cracked beam element model on really thin-walled box beams, it can be anticipated that the basic model error associated with the Timoshenko beam representation of the beam will increase due to the increased contribution of in-plane deformations. Nevertheless, similar to the situation with the thick-walled box sections, by employing the relative shift measure of the modal properties with respect to the intact beam under the same model, the basic model error could be neutralised to a large extent. As such, the cracked beam element model could be similarly effective in the identification of the cracks in thin-walled box beams. This is illustrated in what follows.

The same square box beam as shown in Fig. 6 is used in the verification. But now a much thinner wall thickness (t_s = 2 mm) is employed in the beam. So the dimension of the beam becomes $B \times t_s \times L = 100 \times 2 \times 2000$ mm and the t_s/B ratio is 0.02. All the other parameters,

403 including material properties, boundary condition and crack parameters, are left to be the
404 same as the thick-walled beam.

405 The same beam models with 4 intact and 1 cracked Timoshenko beam elements are used
406 to predict the natural frequencies and mode shapes of the thin-walled box beams. The
407 comparison between numerically simulated (with refined FE) and the predicted (using the
408 Timoshenko beam with cracked beam element model) results for the lowest four natural
409 frequencies is shown in Table 3.

410 It can be seen that the cracked beam element model is able to predict the first couple
411 modes of natural frequencies with similar accuracy to those in the thick-walled beams. But for
412 the 3^{rd} and 4^{th} modes, the errors in the predicted results are considerably large (8.2% - 33.9%).
413 As mentioned earlier this is attributable to stronger presence of warping, distortion and shear-
414 lag effects in the thin-walled section.

415 In terms of the relative shifts of the natural frequencies brought by the crack as defined in
416 Eq. (15), however, the results are presented in Fig. 9. It can be seen that the numerically
417 simulated and predicted results have good match for all the modes. It indicates that by
418 calculating the relative shift of frequency, the modelling errors brought by non-classic beam
419 effects can be greatly eliminated and the cracked beam element model is capable of predicting
420 the frequency shifts accurately up to the first four modes for the thin-walled beam.

421 MAC results of the first 4 mode shapes for the thin-walled beam are all greater than 0.997
422 (hence not shown) and this shows the cracked beam element model can predict the mode
423 shapes with high accuracy even though strong non-classic beam effects are presented.

424 The crack damage identification procedure presented in the previous section is
425 subsequently applied on the cracked thin-walled box beams. Model updating results are
426 presented in Fig. 10. It can be seen that the cracked element is identified correctly for both
427 beams (element 2). The updated crack depth ratios have similar accuracy to those for the

thick-walled beams. As for the relative crack location (l_c) within cracked element, the results from the updating are 209mm and 207mm for the two beams, respectively, as compared to the actual 200mm. In combination the results show that the Timoshenko-based cracked beam element model performs well for crack damage identification of both thick-walled and thin-walled box beams.

EXPERIMENTAL VERIFICATION WITH THE CRACKED BEAM ELEMENT MODEL

An experimental programme of modal testing with box-section beams has been conducted to further verify the cracked beam element model for this type of beams. Both single-crack and multiple-crack beams were prepared for the tests to cover different possible crack damage scenarios in box beams.

Test specimens

Five square steel box-section beams with dimension as $B \times t_s \times L = 100 \times 5 \times 1200$ mm were prepared in the modal testing programme, as shown in Fig. 11.

The beams are labelled as H0, H1-H4 in sequential order, with beam H0 being an intact beam as the reference. Beams H1-H4 are cracked beams, and the cracks all propagate into the vertical walls (i.e., having the form shown in Fig. 1(b)). The arrangements of the cracks were made to represent different cracked beam scenarios, including having both single and multiple cracks. Beams H1 and H2 contained a single crack at the same relative location but different crack depth ratios. Beams H3 and H4 have 2 and 3 cracks, respectively. In beam H3, the two cracks are remotely spaced whereas in beam H4, two of the cracks are closely spaced. The cracks were created with saw cuts and the width of the cut is around 1mm. It is worth noting that it is a common practice to create cracks using saw-cut in laboratory studies, and it is generally established that the stress intensity factors for real crack tips are applicable to the

tips of deep slender notches (Tada et al., 2000). Therefore, the cracked beam element model can be applied to the tested specimens with notches directly. Detailed information of the cracks is presented in Table 4.

Modal testing setup

Free-free boundary conditions were created for the tested beam with two strings, as shown in Fig. 12. A precision impact hammer (B & K type 8206-002) was used to excite the beam. The hammer was capable of generating a relatively uniform impact force spectrum in the range of 0-10000 Hz, which was sufficient to cover the first several vibration modes of the beam. The acceleration response of the beam was measured with light-weight accelerometers with a measurement range of ±700 m/s^2 (B & K Delta Tron® 4508 B003 type). The measurements were recorded with a multi-channel data acquisition system (NI-9234). The sampling rates for both excitation and response measurements were set to be 25600 Hz which was dictated by the small pulse duration of the impact force, and the record duration of the signals were set to be 16 s, which was long enough to cover the entire transient vibration.

Both the natural frequencies and mode shapes of the beams were measured during the modal testing. To extract the mode shapes, 11 uniformly distributed measurement locations were marked on the beam, as shown in Fig. 12(b). An accelerometer was attached at location P4 while another one was attached to the bottom side of the beam at the same span location. The reason for such arrangement was primarily to enable the identification of global bending modes and a detailed explanation will be given in the next sub-section. During the tests, impact was applied at each measurement location from P1 to P11 in a routine procedure.

Frequency response function (FRF) curves were calculated with the Fourier transform of the impact force and acceleration signals. To reduce the measurement noises in the FRFs, general signal processing techniques such as windowing and averaging were applied. A force window was employed on the measured the impact force signal, and 10 repetitive tests were

477 performed for each excitation location and the obtained FRF curves were averaged to get the
478 final FRF.

479 **Modal testing results**

480 A representative measured FRF curve from the intact beam H0 is shown in Fig. 13. It can
481 be seen that the curve is of good quality and has clear resonances. The natural frequencies and
482 mode shapes of the beam can be extracted from the FRF curve in a rather straightforward
483 manner.

484 It should be noted that there are some 11 resonances in the frequency range of 1000-2000
485 Hz, but not all these resonances belong to transverse bending modes. To identify from the
486 modal testing results the transverse bending modes, which are the modes used for crack
487 identification with the Timoshenko-cracked beam element model, the mode shapes need to be
488 employed to distinguish these modes from the local modes.

489 It has been mentioned in the previous sub-section that two accelerometers were attached
490 at both sides of the tested beam, so two sets of mode shapes were obtained for the beams. For
491 a global transverse bending mode, the mode shapes extracted from the top and bottom
492 accelerometers should match each other consistently. To assist in a more precise identification
493 process, the Timoshenko beam element model is used to provide an approximate prediction of
494 the transverse bending mode shapes and calculate the MAC values between the predicted and
495 measured modes. The measured modes which give high MAC values can be identified as real
496 bending modes (herein a MAC of 0.95 is used as a threshold).

497 It is found that basically there are three types of modes in the FRF curves, and the
498 corresponding measured mode shape displacements are shown in Fig. 14, where x is the beam
499 span location. The curves shown in Fig. 14(a) are not correlated to any bending mode and can
500 be easily discarded. The curves in Fig. 14(b) show good match with each other. After
501 comparing with the predicted modes, it is confirmed that this is the 2nd bending mode for the

beam. The two curves in Fig. 14(c) also show good correlation with the predicted mode shape (1st mode). However, it is noted that the mode shapes from the two accelerometers have opposite bending directions. In other words, it is not a global bending mode, but a mode associated with the vibration of box walls. This kind of wall vibration modes has been observed and discussed in the literature (e.g. Hung et al. 1995) and should as well be discarded.

With the above process, the lowest 3 bending modes of the tested box beams can be separated, as shown in Fig. 13. The extracted natural frequencies and displacement-normalized 1st mode shapes for all the five beams are shown in Table 5-6 and Fig. 15.

Verification of the prediction of modal properties by the cracked beam element

Beam models with the cracked beam element are used to predict the natural frequencies and mode shapes of the tested beams. The beam models include 6 beam elements with uniform length as 200 mm. The elastic modulus of the steel beams was confirmed from a preliminary updating and the result indicates this was 208 GPa.

Comparison of measured and predicted natural frequencies are shown in Table 5 and 6. It can be seen that similar to the observation in the sub-section "Vibration analysis with the cracked beam element", the beam models are able to predict the frequencies of lower modes with good accuracy but the errors in the 3rd mode frequency are considerably large, for reasons explained before. Nevertheless, the predicted frequency shifts of the first three modes of beams with a single crack (beam H1 and H2) match very well with the measured results, as shown in Fig. 16. For the beams with multiple cracks, the frequency shifts of the first couple of modes also match well. For the 3rd mode, the errors are higher than those of single crack beams. One explanation is that the presence of a crack alters the effect of shear lag on the beam behaviour and with multiple cracks the deviation from a standard Timoshenko beam is amplified.

MAC results between the measured and predicted mode shapes are shown in Table 7. The MAC values are close to 1 for the first two modes of all beams. For beams with multiple cracks, the MAC values are slightly lower but still exceed 0.95.

Model updating and crack damage identification

The model updating strategy presented in the numerical verification section is applied on the tested beams to identify the cracks. The beam models contain 6 equal-length beam elements but the two free end elements are excluded from the updating to avoid ill-conditioning. So totally there are 8 updating parameters. The actual crack parameters for the beams are listed here for the later comparison with the (inverse) updating results. For beam H1, the crack is in the 4th element with [α, l_c]= [0.79, 150]; for beam H2, the crack is in the 3rd element with [α, l_c]= [1.01, 50]; for beam H3, the cracks are in the 3rd and 5th elements, with [α, l_c]= [0.94, 20] and [0.74, 70], respectively; for beam H4, the cracks are in the 2nd, 4th and 5th elements with [α, l_c]= [0.99, 90], [0.68, 180] and [0.84, 60], respectively. The measured first 3 modes of natural frequencies and mode shapes are used to form the objective function with Eq. (17) and GA is employed to search for the optimistic solution.

The updated results are presented in Table 8 and Fig. 17. It can be seen that the correct crack element number can be identified for both the single-crack and multiple-crack beams. Compared with the actual crack conditions shown in Fig. 11 and summarized above, it is found that the updated crack depth ratios and locations have very good accuracy. The crack depth ratios (α) generally have errors lower than 6% except the one in the 3rd element of beam H3 (with error as 13%). Errors in the crack locations (l_c) are all smaller than 15%. It is noted that a marked false crack is identified in the 5th element in beam H2 and in the 2nd element in beam H2 and H3. As explained earlier, this is partly attributed to the low sensitivity of elements close to the beam end to the modal information, and partly due to measurement

551 errors in modal testing results and modelling errors in the beam element model. Overall, the
552 crack identification with the cracked beam element is deemed as successful for both the
553 single-crack and multiple-crack beams.

554 ## CONCLUSIONS

555 A cracked beam element model has been developed for the crack damage identification
556 of box-section beams. The model is formulated taking into account the additional flexibility
557 brought by the crack, using Timoshenko beam as the base element. The additional flexibility
558 is established in accordance with the fracture mechanics theory. Shear deformation and
559 coupling between transverse and longitudinal DOFs are also represented in the model. To
560 calculate the additional flexibility matrix, the stress intensity factors for cracked box-section
561 beams have been derived from an empirical approach combining FE simulation, parametric
562 analysis and regression.

563 The cracked beam element model has been verified against numerically simulated modal
564 data. Results show that the model is capable of predicting the natural frequencies of the
565 lowest modes with high accuracy but larger errors incur for higher modes, especially for thin-
566 walled beams. However, the modelling errors can be largely neutralised when the relative
567 shift of the frequency is calculated. The mode shapes can also be predicted with good
568 accuracy. The cracked beam element model was then employed in a crack identification
569 process via finite element model updating. Results show that the cracks can be identified with
570 high accuracy for both the thick-wall and thin-wall beams.

571 The cracked beam element model was subsequently verified against experimentally
572 measured modal data. Different crack scenarios with both single-crack and multiple-crack
573 were created in the tested beams. Modal test was carried out on the box beams to extract the
574 natural frequencies and mode shapes. The first three bending modes were extracted from the
575 measurements. Comparison between the measured and predicted natural frequency shifts as

well as mode shapes showed good accuracy for both the single-crack and multiple-crack beams. Crack identification results have also shown that correct cracks can be identified for both single-crack and multiple-crack beams. The updated crack depth and relative crack position within the cracked element generally have achieved good accuracy.

The outcome from this study paves a way for the extension of the cracked beam element model to other types of cross-sections for the crack damage identification purposes.

ACKNOWLEDGEMENTS

The research reported in the paper is partly funded by the Chinese Scholarship Council and the University of Edinburgh through a joint scholarship for the PhD study of the first author.

APPENDIX

The stress intensity factors (SIF) for square box beams of uniform wall thickness (t_s) can be expressed as follows.

For cracks at stage 1:

$$K_{\mathrm{I1}}^{\mathrm{H}} = \frac{N}{A_0}\sqrt{\pi a_{\mathrm{H}}}\,F_{\mathrm{I1}}^{\mathrm{H}}\left(a_{\mathrm{H}}/B, t_{\mathrm{s}}/B\right)$$

$$\text{where, } F_{\mathrm{I1}}^{\mathrm{H}}\left(a_{\mathrm{H}}/B, t_{\mathrm{s}}/B\right) = m\left(a_{\mathrm{H}}/B\right)\cdot\left(t_s/B\right) + n\left(a_{\mathrm{H}}/B\right)$$

$$m\left(a_{\mathrm{H}}/B\right) = -0.975 - 1.341\left(a_{\mathrm{H}}/B\right) + 17.283\left(a_{\mathrm{H}}/B\right)^2 - 83.681\left(a_{\mathrm{H}}/B\right)^3 + 111.982\left(a_{\mathrm{H}}/B\right)^4$$

$$n\left(a_{\mathrm{H}}/B\right) = 1.011 - 0.092\left(a_{\mathrm{H}}/B\right) + 0.572\left(a_{\mathrm{H}}/B\right)^2 + 5.989\left(a_{\mathrm{H}}/B\right)^3 - 9.190\left(a_{\mathrm{H}}/B\right)^4$$

$$K_{\mathrm{I2}}^{\mathrm{H}} = \frac{MB}{2I}\sqrt{\pi a_{\mathrm{H}}}\,F_{\mathrm{I2}}^{\mathrm{H}}\left(a_{\mathrm{H}}/B, t_{\mathrm{s}}/B\right)$$

596 $$\text{where, } F_{I2}^{H}\left(a_H/B, t_s/B\right) = m\left(a_H/B\right)\cdot\left(t_s/B\right) + n\left(a_H/B\right)$$

597 $$m\left(a_H/B\right) = -1.885 - 3.596\left(a_H/B\right) + 31.962\left(a_H/B\right)^2 - 131.227\left(a_H/B\right)^3 + 156.844\left(a_H/B\right)^4$$

598 $$n\left(a_H/B\right) = 1.0013 - 0.0078\left(a_H/B\right) - 0.0936\left(a_H/B\right)^2 + 7.8811\left(a_H/B\right)^3 - 10.9710\left(a_H/B\right)^4$$

599 For cracks at stage 2:

600 $$K_{I1}^{V} = \frac{N}{A_0}\sqrt{\pi a_V}\,F_{I1}^{V}\left(a_V/B, t_s/B\right)$$

601 $$\text{where, } F_{I1}^{V}\left(a_V/B, t_s/B\right) = m\left(a_V/B\right)\cdot\left(t_s/B\right) + n\left(a_V/B\right)$$

602 $$m\left(a_V/B\right) = -7.407 + 36.068\left(a_V/B\right) - 137.172\left(a_V/B\right)^2 + 241.490\left(a_V/B\right)^3 - 162.964\left(a_V/B\right)^4$$

603 $$n\left(a_V/B\right) = 5.346 - 23.645\left(a_V/B\right) + 105.557\left(a_V/B\right)^2 - 192.984\left(a_V/B\right)^3 + 152.806\left(a_V/B\right)^4$$

604 $$K_{I2}^{V} = \frac{MB}{2I}\sqrt{\pi a_V}\,F_{I2}^{V}\left(a_V/B, t_s/B\right)$$

605 $$\text{where, } F_{I2}^{V}\left(a_V/B, t_s/B\right) = m\left(a_V/B\right)\cdot\left(t_s/B\right) + n\left(a_V/B\right)$$

606 $$m\left(a_V/B\right) = -12.151 + 57.042\left(a_V/B\right) - 215.499\left(a_V/B\right)^2 + 376.957\left(a_V/B\right)^3 - 267.067\left(a_V/B\right)^4$$

607 $$n\left(a_V/B\right) = 5.269 - 24.092\left(a_V/B\right) + 100.185\left(a_V/B\right)^2 - 182.504\left(a_V/B\right)^3 + 138.946\left(a_V/B\right)^4$$

608 $$K_{II}^{V} = \frac{P}{A_e}\sqrt{\pi a_V}\,F_{II}^{V}\left(a_V/B, t_s/B\right)$$

609 $$\text{where, } F_{II}^{V}\left(a_V/B, t_s/B\right) = m\left(a_V/B\right)\cdot\left(t_s/B\right)^2 + + n\left(a_V/B\right)\cdot\left(t_s/B\right) + p\left(a_V/B\right)$$

610 $$m\left(a_V/B\right) = -42.923 - 748.211\left(a_V/B\right) + 6810.320\left(a_V/B\right)^2 - 17903.959\left(a_V/B\right)^3 + 15145.796\left(a_V/B\right)^4$$
611

612 $$n\left(a_V/B\right) = -16.369 + 359.143\left(a_V/B\right) - 2115.288\left(a_V/B\right)^2 + 4824.795\left(a_V/B\right)^3 - 3810.311\left(a_V/B\right)^4$$

613

614 $$p\left(a_V/B\right) = 2.514 - 14.370\left(a_V/B\right) + 82.745\left(a_V/B\right)^2 - 177.632\left(a_V/B\right)^3 + 136.118\left(a_V/B\right)^4$$

615

616

617 **REFERENCES**

618 Carpinteri, A., Paggi, M., and Pugno, N. (2006). "Numerical evaluation of generalized stress-
619 intensity factors in multi-layered composites." *Int. J. Solids Struct.*, 43(3-4), 627-641.

620 Carrera, E., Giunta, G., and Petrolo, M. (2011). *Beam structures: Classical and advanced*
621 *theories*, John Wiley & Sons, USA.

622 Carrera, E., and Varello, A. (2012). "Dynamic response of thin-walled structures by variable
623 kinematic one-dimensional models." *J. Sound Vib.*, 331(24), 5268-5282.

624 Cerri, M. N., and Vestroni, F. (2003). "Use of frequency change for damage identification in
625 reinforced concrete beams." *J. Vib. Control*, 9(3-4), 475-491.

626 Cowper, G. (1966). "The shear coefficient in Timoshenko's beam theory." *J. Appl. Mech.*,
627 33(2), 335-340.

628 Doebling, S. W., Farrar, C. R., Prime, M. B., and Shevitz, D. W. (1996). *Damage*
629 *identification and health monitoring of structural and mechanical systems from changes*
630 *in their vibration characteristics: A literature review*, Los Alamos National Lab., NM
631 (USA).

632 Dunn, M. L., Suwito, W., and Hunter, B. (1997). "Stress intensity factors for cracked I-
633 beams." *Eng. Fract. Mech.*, 57(6), 609-615.

634 Gao, H., and Herrmann, G. (1992). "On estimates of stress intensity factors for cracked beams
635 and pipes." *Eng. Fract. Mech.*, 41(5), 695-706.

636 Hou, C. C., and Lu. Y. (2016). "Identification of cracks in thick beams with a cracked beam
637 element model" *J. Sound Vib.*, http://dx.doi.org/ 10.1016/j.jsv.2016.09.009.
638 Hu, N., Wang, X., Fukunaga, H., Yao, Z. H., Zhang, H. X., and Wu, Z. S. (2001). "Damage
639 assessment of structures using modal test data." *Int. J. Solids Struct.*, 38(18), 3111-3126.
640 Hung, K. C., Liew, K. M., and Lim, M. K. (1995). "Free-vibration of cantilevered cylinders -
641 effects of cross-sections and cavities." *Acta Mech.*, 113(1-4), 37-52.
642 Jones, K., and Turcotte, J. (2002). "Finite element model updating using antiresonant
643 frequencies." *J. Sound Vib.*, 252(4), 717-727.
644 Kim, Y. Y., and Kim, J. H. (1999). "Thin-walled closed box beam element for static and
645 dynamic analysis." *Int. J. Numer. Meth. Eng.*, 45(4), 473-490.
646 Liu, A. (1996). *Summary of stress-intensity factors*, ASM International, Member/Customer
647 Service Center, Materials Park, OH 44073-0002, USA, 1996., 980-1000.
648 Liu, D., Gurgenci, H., and Veidt, M. (2003). "Crack detection in hollow section structures
649 through coupled response measurements." *J. Sound Vib.*, 261(1), 17-29.
650 Lu, Y., and Tu, Z. G. (2004). "A two-level neural network approach for dynamic FE model
651 updating including damping." *J. Sound Vib.*, 275(3-5), 931-952.
652 Luo, Q., Li, Q., and Tang, J. (2002). "Shear lag in box girder bridges." *J. Bridge Eng.*,
653 10.1061/(ASCE)1084-0702(2002)7:5(308), 308-313.
654 Moaveni, B., He, X., Conte, J. P., and De Callafon, R. A. (2008). "Damage identification of a
655 composite beam using finite element model updating." *Comput. Aided Civ. Infrastruct.*
656 *Eng.*, 23(5), 339-359.
657 Mottershead, J. E., and Friswell, M. I. (1993). "Model updating in structural dynamics - a
658 survey." *J. Sound Vib.*, 167(2), 347-375.
659 Nussbaumer, A. C., Fisher, J. W., and Dexter, R. J. (1999). "Behavior of long fatigue cracks
660 in cellular box beam." *J. Struct. Eng.*, 10.1061/(ASCE)0733-9445(1999)125:11(1232),

661 1232-1238.
662 Perera, R., and Torres, R. (2006). "Structural damage detection via modal data with genetic
663 algorithms." *J. Struct. Eng.*, 10.1061/(ASCE)0733-9445(2006)132:9(1491), 1491-1501.
664 Reissner, E. (1946). "Analysis of shear lag in box beams by the principle of minimum
665 potential energy." *Q. Appl. Math.*, 5(3), 268-278.
666 Sohn, H., Farrar, C. R., Hemez, F. M., Shunk, D. D., Stinemates, D. W., Nadler, B. R., and
667 Czarnecki, J. J. (2004). *A review of structural health monitoring literature: 1996-2001*,
668 Los Alamos National Laboratory Los Alamos, NM (USA).
669 Tada, H., Paris, P. C., and Irwin, G. R. (2000). *The stress analysis of cracks handbook*, The
670 American Society of Mechanical Engineers. New York.
671 Tu, Z. G., and Lu, Y. (2008). "FE model updating using artificial boundary conditions with
672 genetic algorithms." *Comput. Struct.*, 86(7-8), 714-727.
673 Unger, J. F., Teughels, A., and De Roeck, G. (2006). "System identification and damage
674 detection of a prestressed concrete beam." *J. Struct. Eng.*, 10.1061/(ASCE)0733-
675 9445(2006)132:11(1691), 1691-1698.
676 Vlasov, V. (1961). *Thin-walled elastic beams*, Israel Program for Scientific Translations.
677 Jerusalem, Israel.
678 Wang, D. A., Lin, P. C., and Pan, J. (2005). "Geometric functions of stress intensity factor
679 solutions for spot welds in lap-shear specimens." *Int. J. Solids Struct.*, 42(24-25), 6299-
680 6318.
681 Xie, Y. J., Wang, X. H., and Lin, Y. C. (2004). "Stress intensity factors for cracked
682 rectangular cross-section thin-walled tubes." *Eng. Fract. Mech.*, 71(11), 1501-1513.
683 Zhang, S. H., and Lyons, L. P. R. (1984). "A thin-walled box beam finite-element for curved
684 bridge analysis." *Comput. Struct.*, 18(6), 1035-1046.
685 Zhang, Y. H., and Lin, L. X. (2014). "Shear lag analysis of thin-walled box girders adopting

686 additional deflection as generalized displacement." *J. Eng. Mech.*,
687 10.1061/(ASCE)EM.1943-7889.0000705, 04014005.
688 Zheng, D. Y., and Fan, S. C. (2003). "Vibration and stability of cracked hollow-sectional
689 beams." *J. Sound Vib.*, 267(4), 933-954.
690 Zhou, S. J. (2010). "Finite Beam Element Considering Shear-Lag Effect in Box Girder." *J.*
691 *Eng. Mech.*, 10.1061/(ASCE)EM.1943-7889.0000156, 1115-1122.

Tables

Table 1. Cantilever box beams with t_s/B= 0.1 (Unit: Hz)

Mode	Intact			Cracked (α_V = 0.3)			Cracked (α_V = 0.5)		
	Simulated	Predicted	ε/%	Simulated	Predicted	ε/%	Simulated	Predicted	ε/%
1	25.9	26.0	**0.4**	23.8	24.1	**1.2**	21.1	21.4	**1.2**
2	157.5	158.3	**0.5**	154.0	155.4	**0.9**	149.8	151.6	**1.2**
3	421.3	427.7	**1.5**	388.7	402.8	**3.6**	356.6	373.7	**4.8**
4	776.6	809.0	**4.2**	767.2	802.7	**4.6**	763.0	799.2	**4.7**

Table 2. Parametric settings for GA

Parameter	Setting
Population size	3000
Fitness limit	-Infinite
Max generation	1500
Crossover fraction	0.7
Mutation rate	0.02

Table 3. Cantilever thin-walled box beams with t_s/B= 0.02 (Unit: Hz)

Mode	Intact			Cracked (α_V = 0.3)			Cracked (α_V = 0.5)		
	Simulated	Predicted	ε/%	Simulated	Predicted	ε/%	Simulated	Predicted	ε/%
1	28.2	28.1	**0.0**	25.5	25.5	**0.0**	22.5	22.6	**0.0**
2	168.7	170.4	**1.0**	164.3	166.4	**1.3**	159.9	162.4	**1.6**
3	422.8	457.7	**8.2**	390.8	424.8	**8.7**	362.6	394.1	**8.7**
4	642.9	860.6	**33.9**	641.6	853.2	**33.0**	641.1	849.6	**32.5**

Table 4. Crack depth and location information

Beam label	Crack1		Crack2		Crack3	
	L_c/mm	α (α_V)	L_c/mm	α (α_V)	L_c/mm	α (α_V)
H0	-	-	-	-	-	-
H1	750	0.79 (0.29)	-	-	-	-
H2	450	1.01 (0.51)	-	-	-	-
H3	420	0.94 (0.44)	870	0.74 (0.24)	-	-
H4	290	0.99 (0.49)	780	0.68 (0.18)	860	0.84 (0.34)

Table 5. Measured and predicted natural frequencies of beams H0, H1 and H2 (Unit: Hz)

Mode	H0			H1			H2		
	Measured	Predicted	ε/%	Measured	Predicted	ε/%	Measured	Predicted	ε/%
1	466.9	466.9	**0.0**	385.4	390.6	**1.3**	305.6	306.3	**0.2**
2	1112.4	1176.7	**5.8**	1010.6	1075.7	**6.4**	954.4	1000.8	**4.9**
3	1701.6	2107.6	**23.9**	1679.5	2106.5	**25.4**	1666.3	2096.8	**25.8**

Table 6. Measured and predicted natural frequencies of beams H3 and H4 (Unit: Hz)

Mode	H3			H4		
	Measured	Predicted	ε/%	Measured	Predicted	ε/%
1	334.0	329.8	**-1.3**	339.0	334.6	**-1.3**
2	817.6	844.9	**3.3**	677.6	706.0	**4.2**
3	1585.7	1763.1	**11.2**	1341.4	1508.4	**12.4**

Table 7. MAC results between measured and predicted mode shapes

Mode	H0	H1	H2	H3	H4
1	1.000	0.998	0.998	0.999	0.999
2	0.999	0.997	0.998	0.997	0.998
3	0.996	0.996	0.973	0.951	0.963

Table 8. Model updating results of crack locations l_c (Unit: mm)

Element number	1	2	3	4	5	6
H1	-	-	-	150 (150)	-	-
H2	-	-	63 (50)	-	-	-
H3	-	-	50 (20)	-	46 (70)	-
H4	-	89 (90)	-	170 (180)	77 (60)	-

Note: the values in the parentheses are actual crack locations.

Figures

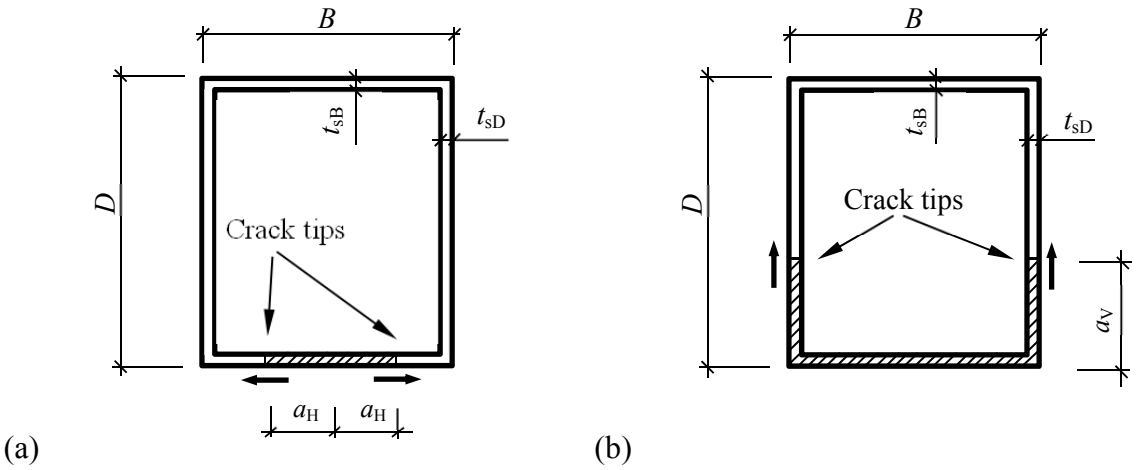

Fig. 1. Crack development of box beam section. (a) Stage 1; (b) Stage 2.

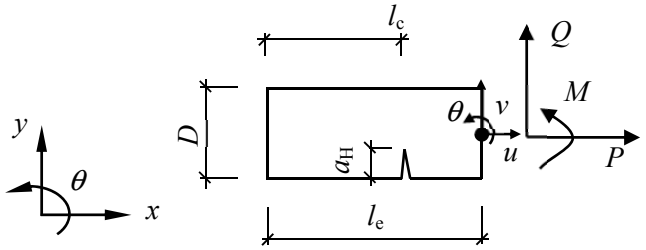

Fig. 2. A cracked beam element

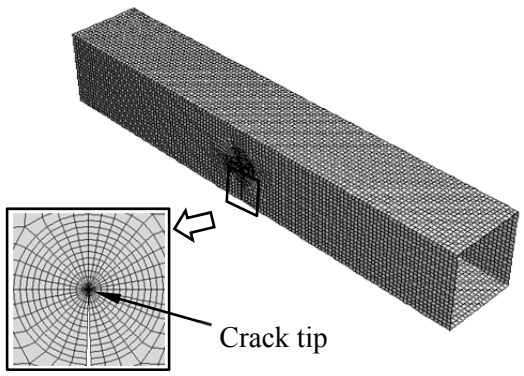

Fig. 3. FE model of the cracked box beam

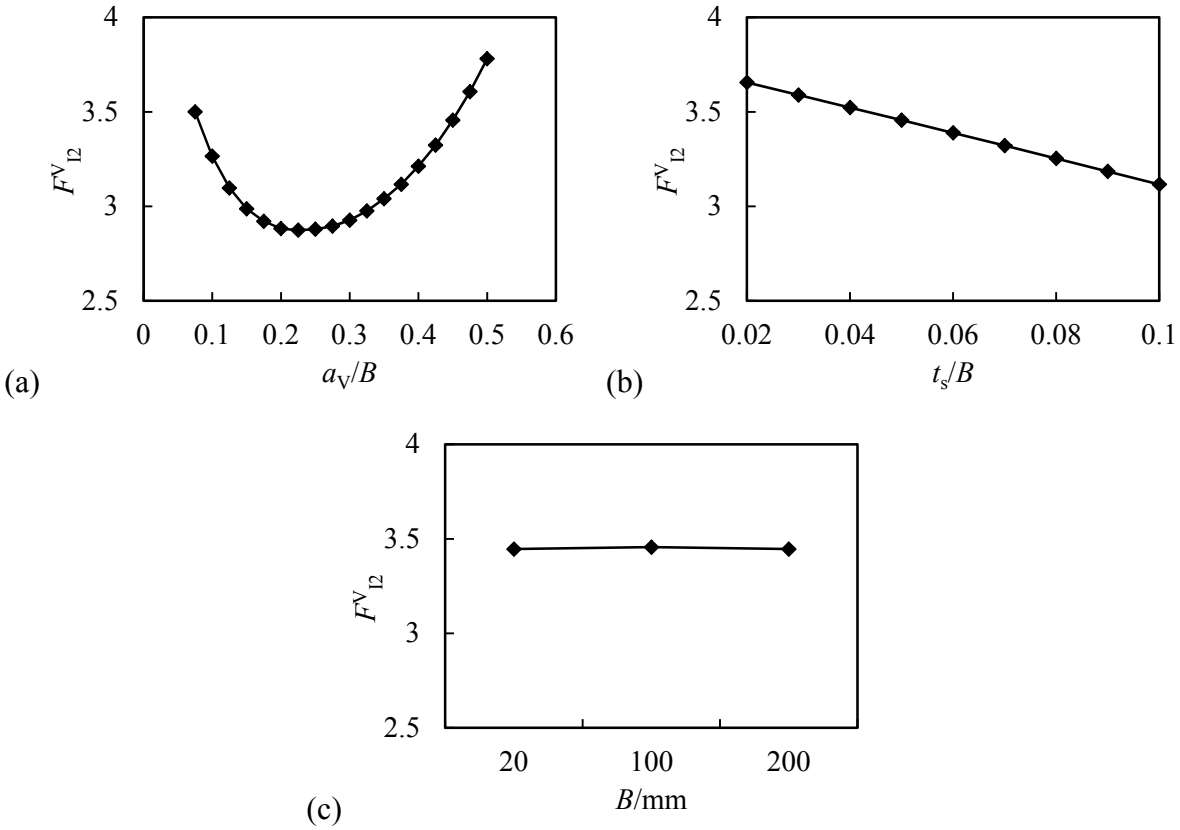

Fig. 4. Parametric study results for F^{V}_{I2}. (a) F^{V}_{I2} versus a_V/B (t_s/B = 0.05, B = 100 mm); (b) F^{V}_{I2} versus t_s/B (a_V/B = 0.45, B = 100 mm); (c) F^{V}_{I2} versus B (t_s/B = 0.05, a_V/B = 0.45).

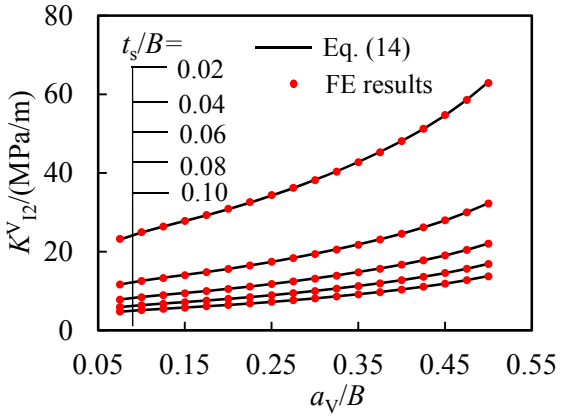

Fig. 5. Comparison of K^{V}_{I2} from FE modelling and Eq. (14)

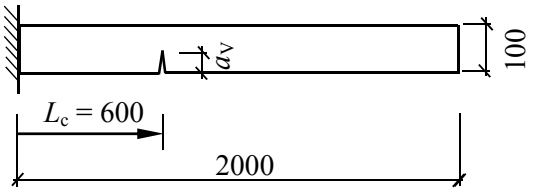

Fig. 6. Schematic of numerically simulated beam (Unit: mm)

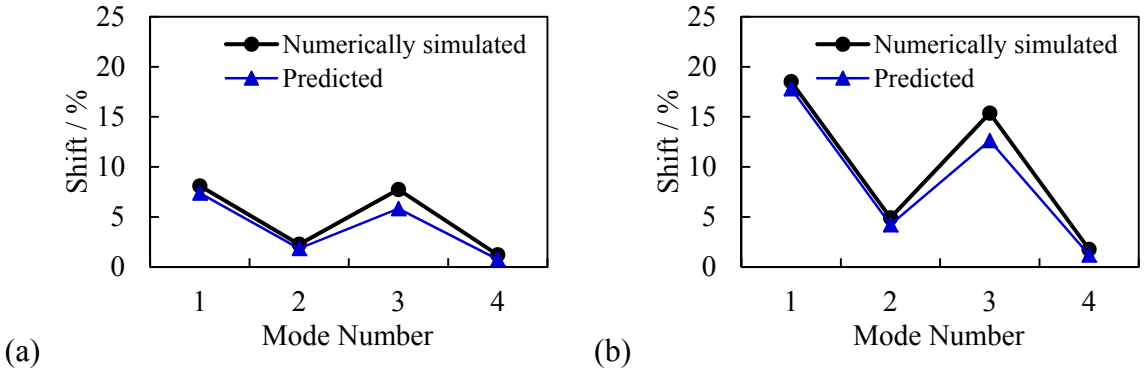

Fig. 7. Comparisons between numerically simulated and predicted frequency shifts for a thick-walled box beam (t_s/B= 0.1) for two crack scenarios: (a) α = 0.8; (b) α = 1.0.

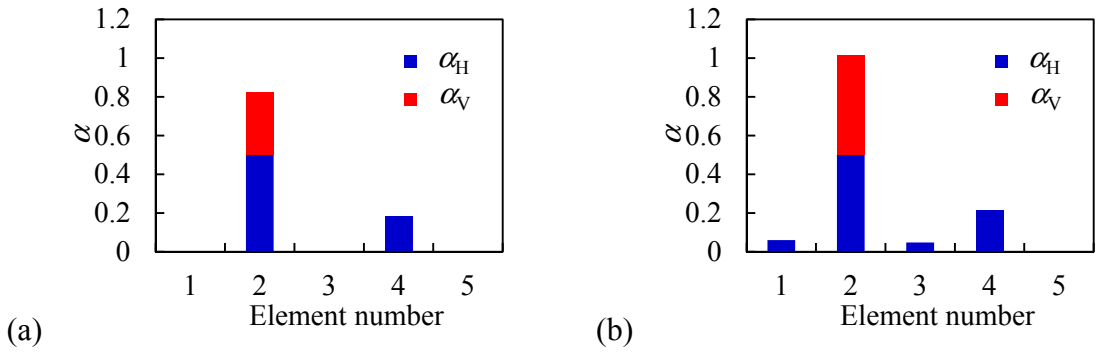

Fig. 8. Updated crack depth ratios (α) of a thick box beam (t_s/B = 0.1) for two crack scenarios: (a) α = 0.8; (b) α = 1.0.

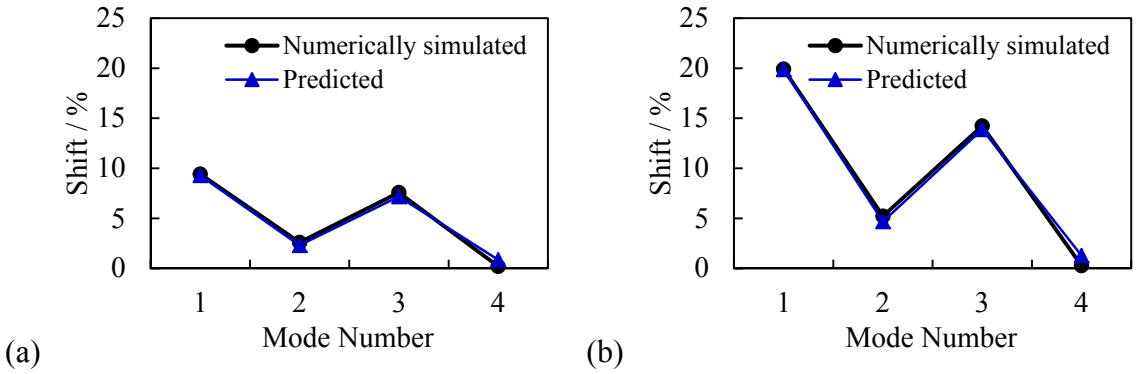

Fig. 9. Comparisons between numerically simulated and predicted frequency shifts for a thin-walled box beam ($t_s/B = 0.02$) for two crack scenarios: (a) $\alpha = 0.8$; (b) $\alpha = 1.0$.

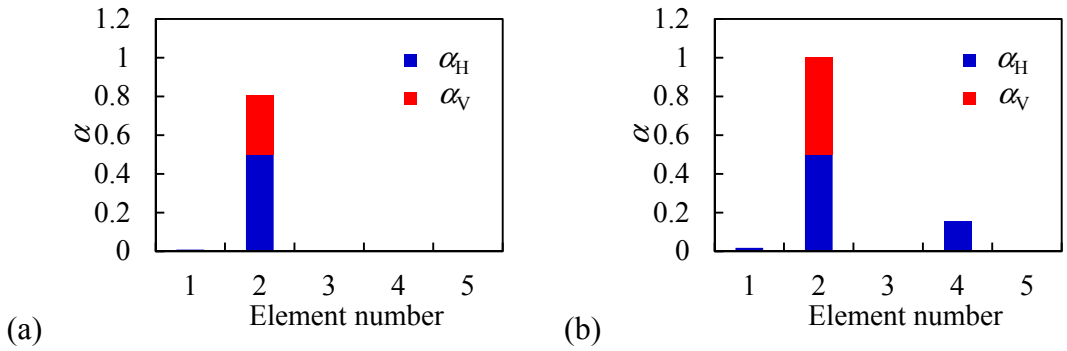

Fig. 10. Updated crack depth ratios (α) of thin-walled box beams ($t_s/B = 0.02$): (a) $\alpha = 0.8$; (b) $\alpha = 1.0$.

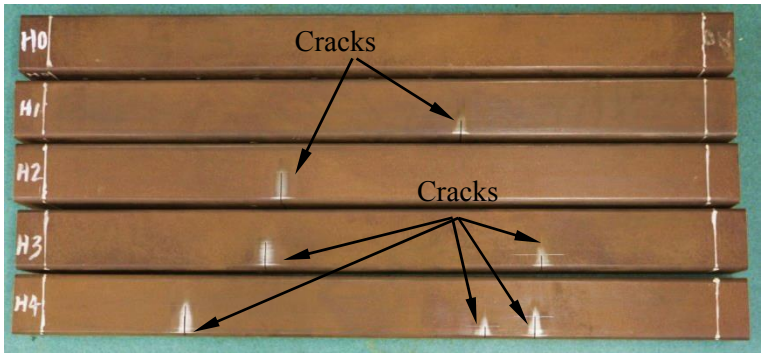

Fig. 11. Experimental box beam specimens

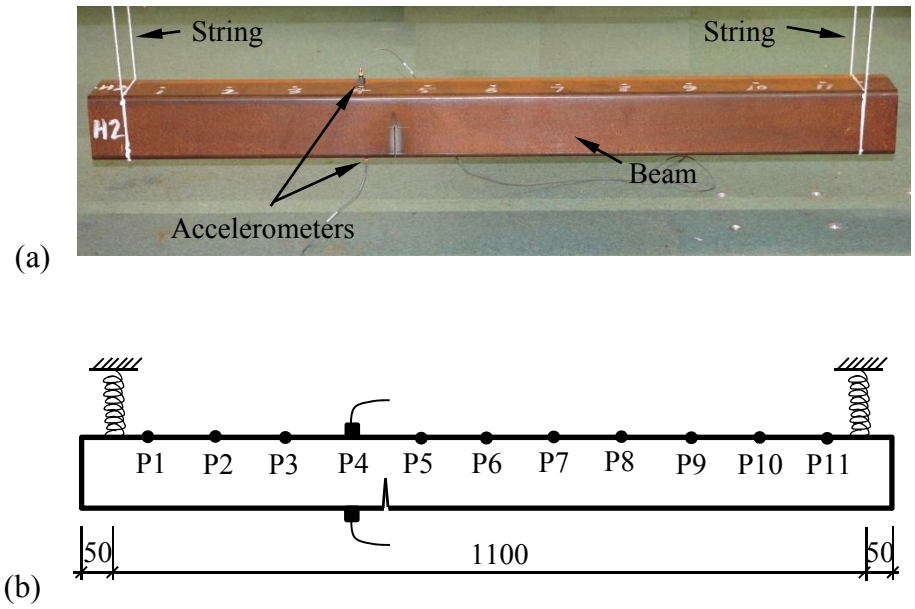

Fig. 12. Modal testing setup. (a) Photo of the setup; (b) Schematic view of the setup (Unit: mm).

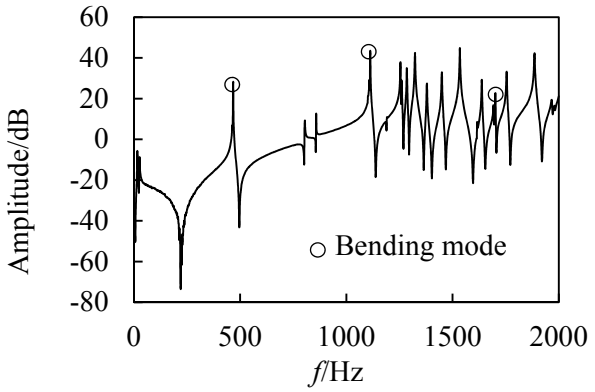

Fig. 13. A typical driving FRF curve (at point P4 of beam H0)

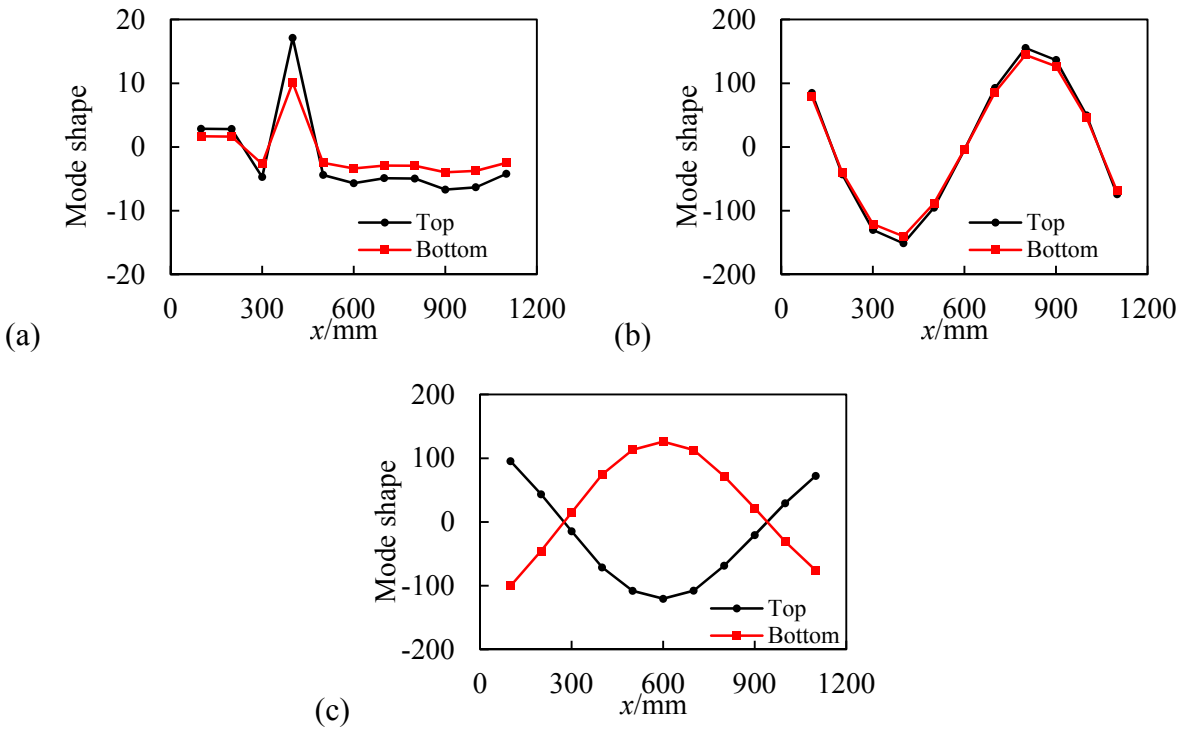

Fig. 14. Comparisons of measured mode shapes from top and bottom accelerometers. (a) Resonance at f = 803.8 Hz; (b) Resonance at f = 1112.4 Hz; (c) Resonance at f = 1284.8 Hz.

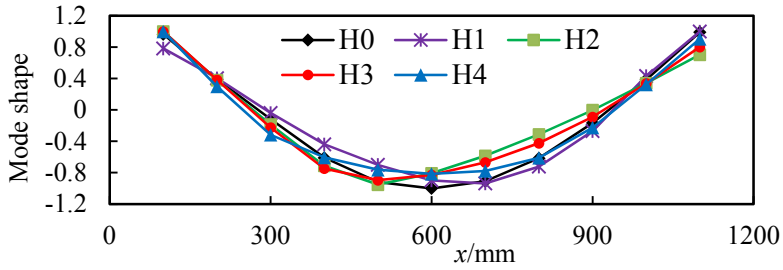

Fig. 15. Measured mode shapes for the first bending mode from all 5 beam specimens

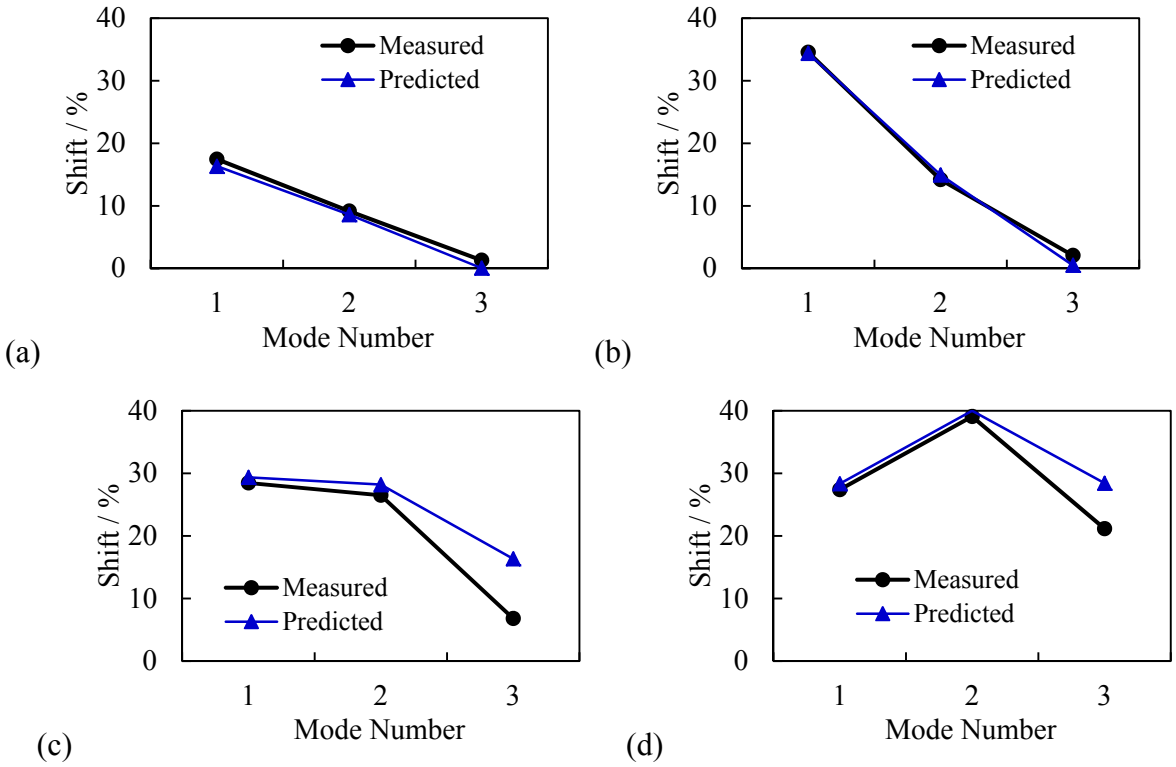

Fig. 16. Comparisons between measured and predicted frequency shifts. (a) H1; (b) H2; (c) H3; (d) H4.

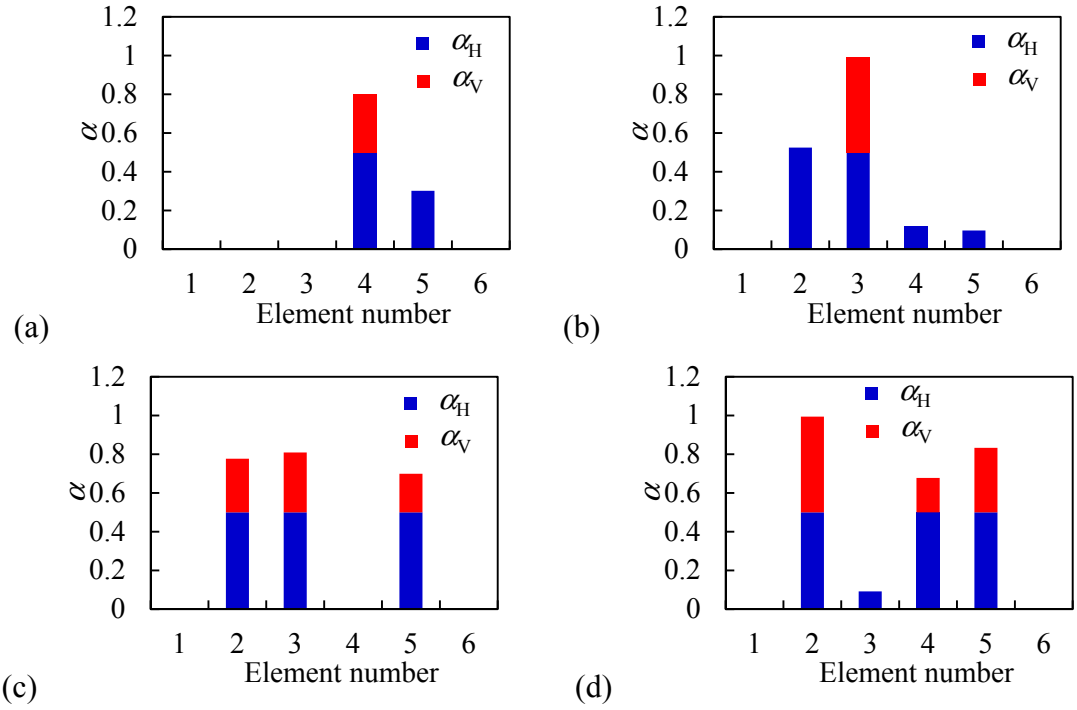

Fig. 17. Model updating results of crack depth ratios α. (a) H1 (4th, α = 0.79); (b) H2 (3rd, α = 1.01); (c) H3 (3rd and 5th, α = 0.94 and 0.74); (d) H4 (2nd, 4th and 5th, α = 0.99, 0.68 and 0.84).